MECHANIKA TEORETYCZNA
I STOSOWANA
Journal of Theoretical
and Applied Mechanics
1, 32, 1994

FRACTURE PROCESS IN REINFORCED CONCRETE BEAMS

LUDOMIR JANKOWSKI

ANDRZEJ PSZONKA

Mechanical Engineering Department

DARIUSZ STYŚ

Civil Engineering Department

Technical University of Wrocław

Crack propagation process in reinforced concrete (RC) beams has been investigated with the aid of acoustic emission (AE) and photoelastic coating methods. Beams with two asymmetric notches were reinforced by a single bar of variable diameter. The "effective" crack length was evaluated due to continuous monitoring of isochromatic fringe patterns and spectrum of the AE signal. Some preliminary results concerning fracture toughness parameters of RC beams have been presented.

1. Introduction

Quasi-elastic fracture mechanics (QEFM), which is often applied to the fracture analysis of concrete-like composites includes physical nonlinearity in the form of the fracture process zone (FPZ) ahead of a crack tip. For homogeneous materials like metals and alloys it is simply a plastic area, for concrete it is a zone of intensive microcracking (MZ). A great part of experimental works in the field of fracture mechanics of concrete is closely related to the problem of FPZ formation.

Detailed characteristics of the experimental methods applied to FPZ detection had been presented by Jankowski and Styś (1990). They are optical methods, ultrasonics techniques, acoustic emission, electric resistant extensometers to mention but a few. Optical techniques cover a photoelastic coating

method, holographic interferometry, moire methods, X – ray radiography and many others.

For metallic specimens transition from plane state of stress at the surface to the plane state of strain inside the specimen results in radical variation of plastic strains in the crack tip region. It is one of the main reasons why the conclusions concerning plastic regions in metals cannot be spread over concrete composites, where the process of microcracks creation dominates over insignificant plastic strains. Comparing FPZ in different concrete specimens (cf Entov and Jagust, 1975; Cedolin et al., 1983; Swartz and Go, 1984) one may notice, that the differences in the range of microcracking zone measured at the surface and inside the specimen, respectively, did not exceed the value of 0.025 m. The crack front becomes more smooth for smaller relative crack length $(a/h < 0.4)$. Similar phenomenon of crack front averaging can be observed in the presence of stress gradient in the cross section containing notch.

Fracture processes in concrete composites are usually analyzed in a static way under fixed grip condition when slow crack growth can be recorded. It is assumed that the fracture process in tensioned area proceeds according to the hypothesis given by Glucklich (1963) and microcracks propagate stepwise primarily along the interphases between cement matrix and aggregates. Microcracks are hampered by the grains of tough gravel what is the main reason for increasing energy demand in the process of new microcracks formation. Mechanism of slow crack growth precedes uncontrolled crack propagation. High – speed photography (cf Jankowski and Styś, 1990) and the AE method (cf Maji and Shah, 1988) confirmed the above mentioned observations. Especially acoustic emission is recently used for the investigation of fracture process in plain concrete and for the localization of cracks in RC specimens (cf Terrien, 1980; Lim and Koo, 1989; Maji et al., 1990; Rossi et al., 1990).

The majority of researches in the field of QEFM of concrete have been conducted on plain concrete specimens. At the next,more complicated step reinforced concrete members should be taken under consideration. At present there is only a few experimental works on fracture behaviour of reinforced concrete. The main reason, which is probably somehow discouraging, is the evidence that the RC beams are known to be fracture insensitive (cf Ingraffea and Saouma, 1986). However, also in this case some modification of the classical fracture toughness parameters are possible (cf Azad et al., 1987). It was also proved that underreinforced RC beams can undergo the fracture collapse (cf Carpinteri, 1986). Standard mode I fracture tests deal with specimens having single, artificial crack acting as a stress concentrator. On the contrary, in RC beams, there are always a few cracks often localized asymmetrically. It

is one of the reasons which calls for modification of test arrangement in the case of RC beams.

Another important problem pertains to the mathematical formulae for calculation of the fracture toughness parameters. They mainly depend on the relative crack length (a/h). Experimental observations confirm that fracture toughness parameters are size-independent, if a "real" or "effective" crack length is used in those formulae (cf Shah and Carpinteri, edit., 1991). That means that "effective" crack lenght should include the range of the fracture process zone ahead of the crack tip. The preliminary results of FPZ investigation via acoustic emission and the photoelastic coating method are presented in this paper. The RC beams with two asymmetric notches were the subject for investigation. The fracture process was monitored during the whole loading spectrum by a video camera for isochromatic fringe patterns registration and acoustic emission sensors for AE signal recording.

2. Description of the experiment

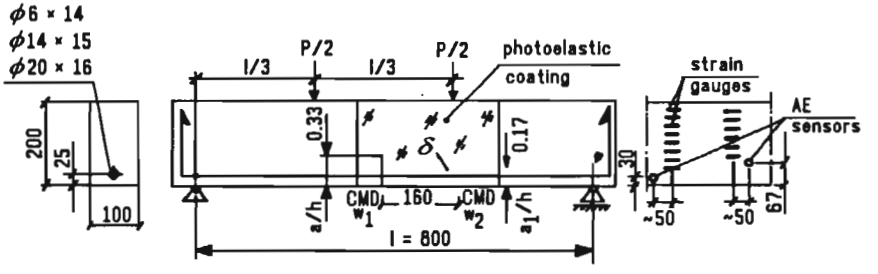

Fig. 1. Basic geometry of the tested beams

The results of three tests performed on concrete beams of dimensions $b \times h \times l = 0.10 \times 0.20 \times 0.80$ m^3 are presented in this paper. In each case the two artificial notches of relative length $a_1/h = 0.33$ and $a_2/h = 0.10$ were moulded. Notches were formed by thin steel plate (0.001 m thick) covered with a silicon separating agent, inserted while casting. Detailed geometry of the beams is shown in Fig.1. Beams had been kept for one year in the conditions of 70% humidity and temperature 15° C. The photoelastic coating 0.002 m thick, prepared on a basis of epoxy resin, was glued on at the midspan. The glue consisted of epoxy resin with modifiers and with alu-

minum powder. Tests were performed according to the four points bending procedure. The UFP 400 testing machine with stroke control and displacement rate 5×10^{-5} m/s was used as a loading set-up. Isochromatic fringe patterns were recorded by video and photo cameras. Crack mouth displacements (CMD) w_1 and w_2 vs. force P were recorded on XY plotters as well as the displacement of the loading point.

Ahead of the crack tip a set of strain gauges was fixed for monitoring strains in the compression zone and for localization of the neutral axis. Acoustic emission was recorded by the two one – channel devices:

first – acoustic emission set-up composed of the processor 201, the preamplifier $60dB$ and the gauge AC 175 L

second – Bruel & Kjaer set-up with the wide – range gauge.

The number of impulses was visualized on a double plotter and AE events were observed on oscilloscope Tektronix 2230 and stored in PC386. At the same time autocorrelation function and AE spectrum were monitored on the Hewlett Packard equipment (correlator 3721A, spectrum analyzer 3720A) and recorded on a double plotter. The elastic modulus of concrete E_s was evaluated by the standard compression test. The value of ultimate tensile strain corresponding to microcrack formation was assumed as $\varepsilon_u = 1.1 \times 10^{-4}$. Material characteristics of photoelastic coating and concrete are given in Table 1.

Table 1

Concrete mix proportions $W:C:S:G$	$d_{\max}$ [mm]	E_s [MPa]	ν_s	E_c [MPa]	ν_c	f_ε [fr. order]$^{-1}$
1:1.7:2.7:5.0	20	28400	0.2	3400	0.38	$1.092 \cdot 10^{-9}$

3. Experimental procedure

The extent of microcracking zone was defined on the basis of isochromatic fringe patterns, employing the fundamental relation between the optical effect and strains

$$\varepsilon_{1c} - \varepsilon_{2c} = \varepsilon_{1s} - \varepsilon_{2s} = N f_\varepsilon \tag{3.1}$$

where

$\varepsilon_1, \varepsilon_2$ – principal strains
c, s – indices, related to the material of coating and specimen, respectively
N – isochromatic fringe order
f_ε – fringe value in terms of strains.

It was additionally assumed, that in the area of pure bending, the Poisson ratio ν_s is determined as follows

$$\frac{\varepsilon_{2s}}{\varepsilon_{1s}} = -\nu_s \tag{3.2}$$

With the relation given above it is possible to define the extent of FPZ boundary on the basis of boundary fringe order N_b, derived from Eq (3.1), having assumed strength hypothesis. It is a matter of convenience to formulate a hypothesis which depends on material characteristics attainable by simple laboratory tests (ultimate stress or strain – σ_u, ε_u). The conditions given by Mazars (1981) and Godycki-Ćwirko (1982) were assumed as a criteria for the FPZ formation, respectively. Strength hypothesis given in terms of stresses yields in this case a simple relation

$$\sigma_1 > \sigma_2 \tag{3.3}$$

The equations of boundary isochromatic fringes and the values of N_b are presented in Table 2.

Table 2

Strength hypothesis	Equation of the boundary fringe pattern	Value of the boundary fringe order N_b
$\sqrt{\varepsilon_1^2 + \varepsilon_2^2} = \varepsilon_u$ where $\varepsilon_2 = \varepsilon_2$ if $\varepsilon_2 > 0$ $\varepsilon_2 = 0$ if $\varepsilon_2 < 0$	$N_b = \frac{\varepsilon_u(1+\nu_s)}{f_\varepsilon}$	0.121 [12]
$\varepsilon_u^2 = \frac{1}{2}(\varepsilon_1^2 + \varepsilon_2^2)$	$N_b = \frac{2\varepsilon_u(1+\nu_s)}{f_\varepsilon\sqrt{1+\nu_s^2}}$	0.168 [6]
$\sigma_1 = \sigma_u$	$N_b = \frac{\sigma_u(1+\nu_s)}{E_s f_\varepsilon}$	0.124

4. Fracture process zone evaluation

On the basis of boundary fringe pattern FEZ were evaluated during the whole loading spectrum. The results of FEZ observations for beam X14 and for both cracks A and B are shown in Fig.2. For each crack, the very moments before and after crack propagation are visualized. Diagram is a linear transformation of the real state with the reducing factor 0.3. Dotted line marks the range of FPZ due to the Mazars criterion. Observations from the three tests give only qualitative description of the fracture process. For the notch, where the first crack propagates the increment of FPZ is very quick and after propagation FPZ starts to diminish and is always smaller, than in the initial uncracked state. Fig.3 shows the history of crack formation for both notches of the beam X14. From the notch B a crack has not been initialized, despite large microcracking area and FPZ increments.

Changes of AE are well correlated with the FPZ development, however they are slightly disturbed by peak-signals due to the crack tip displacement. Function ΔI of the AE intensity measured by the B&K gauge (the area of central crack) is also shown in Fig.2.

The acoustic emission method seems to be more sensitive, and detects earlier the microcracking process than the photoelastic coating method. The FPZ development, which is monotonical in photoelastic observations, appears to be more complicated what reveals acoustic emission. For the final stages of crack propagation friction effects become dominant in the acoustic emission spectrum.

5. Acoustic emission events

Experimental set-up for monitoring of the AE events consisted of the B&K signal analyzer 4429, the amplifier 2638, and the wide range sensor with the built-in preamplifier $40dB$. According to its service characteristics the effective range of signal analysis is from 100 kHz to 1 MHz. Unfortunately, the characteristic of sensor is not flat and shows some resonances in the vicinity of frequencies 270, 620 and 920 kHz. Signals were stored in the memory of the oscilloscope Tektonix 2230 and then transmitted, with a supplementary data, to a PC386 computer for the further "off-line" analysis. Initiating impulse was two times higher than the background level. Every event was analyzed by the numerical procedure PS30, elaborated in the Group of Signals The-

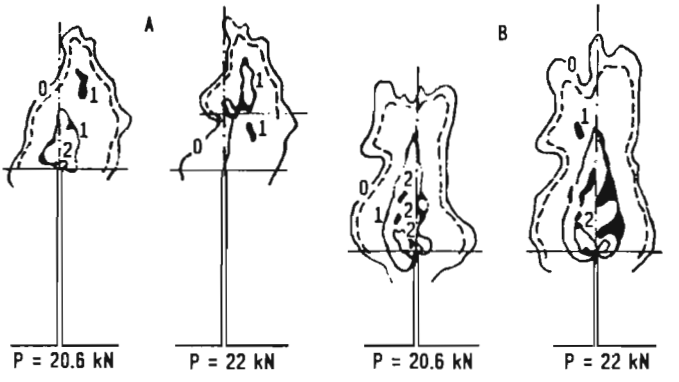

Fig. 2. Isochromatic fringes for the beam X14 at loading stages 20.6 and 22 KN, respectively

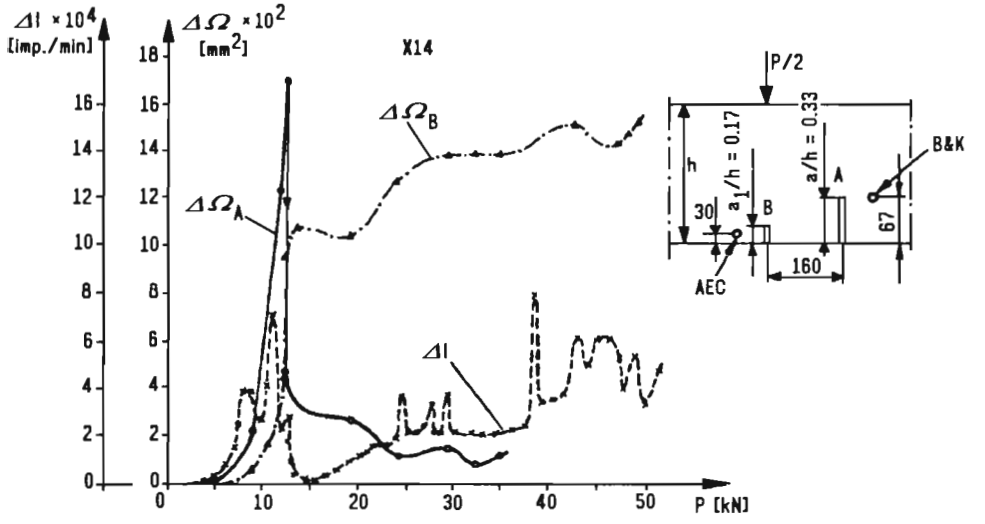

Fig. 3. FPZ evolution for A and B notches of the beam X14

ory – Institute of Telecommunication and Acoustic, Technical University of Wrocław.

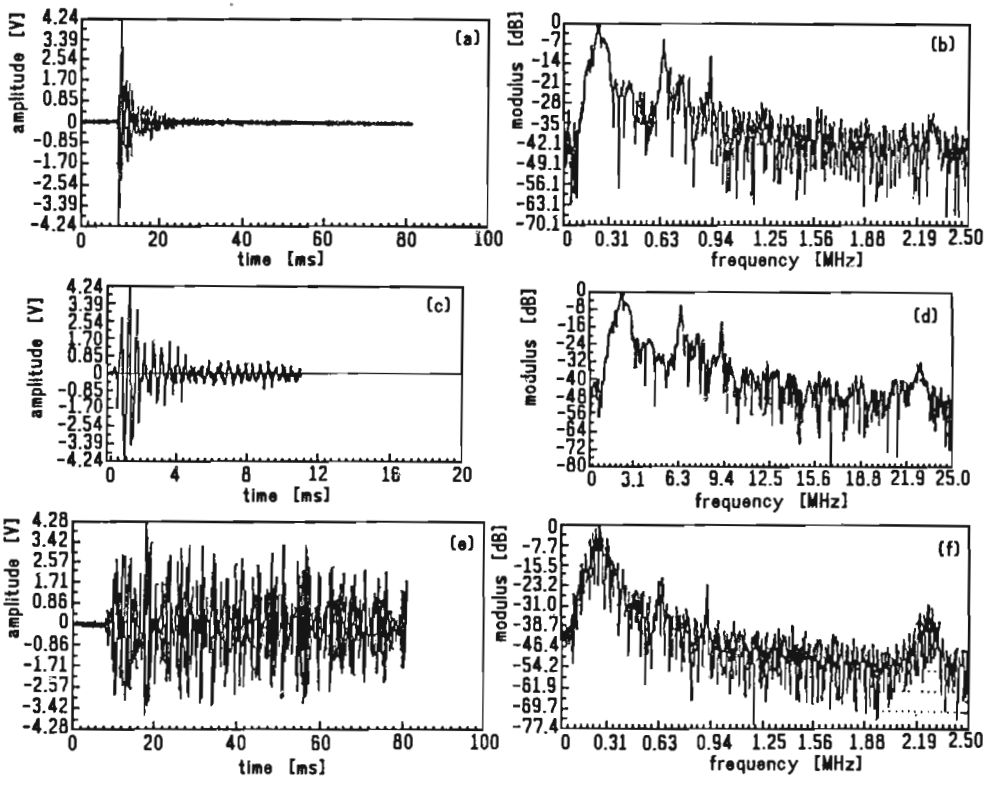

Fig. 4. Examples of the AE events and their harmonic analysis

The AE events were divided into three stages connected with the degradation of the internal structure of concrete, namely: I – crack initiation phase, II – stable crack propagation or slow crack growth, III – final fracture. For the reason that in every case low-frequency peak has been dominating, graphs in Fig.4 are presented in a power scale (dB). Approximately 1000 events have been analyzed. An example of acoustic signal of one event and its spectral analysis are presented in Fig.4a,b. The same case, after removing background peak frequencies, is shown in Fig.4c,d. "The background effect" for the whole series of acoustic events illustrates Fig.4e,f.

Statistical analysis of the spectrum intensity distribution, for all phases of concrete deterioration, does not reveal substantial differences, however,one may observe the domination of low-frequency resonance increasing with the

accumulation of internal defects in concrete microstructure.

In a small group of events resonances appear in various areas of acoustic spectrum. In the phase I – resonance has been observed for 410 kHz, in the phase III – for 780 kHz. Resonance for frequency 390 kHz has equal in probability at every stage of microcracking process. Population of signals with additional resonance frequencies is less than 10 % for every stage.

Distributions of time increasing for particular signals did not show essential in differences at all three stages. The values of time increasing were in the range from 5 to 800 μs, but over 80% of events were located below the level of 120 μs.

6. Spectrum of the AE signal

Investigation of the AE spectrum has been conducted by the B&K equipment and the Hewlett Packard analyzer. HP set-up allows for the analysis of acoustic signal up to the range of 0.5 MHz. AE spectrum has been recorded during all phases of micro and macrocracks propagation via high-pass filter of 200 kHz and for global amplification of $80dB$. Results are presented in Fig.5. Curves (a), (b), and (c) represent initial and advanced microcracking, and the very moment of crack propagation, respectively. The curve (d) represents the second specimen in the crack propagation stage. The reproducibility of results is quite good. Spectrum, which is characteristic for the clear signal created by friction along the specimen surface, is described by the curve (e). Notwithstanding the fact, that AE spectrum depends on many factors, the domination of the first resonance is clearly visible. For making some qualitative observation, it has been found interesting to compare the results recorded on cement mortar specimen. The curve (f) characterizesthe process of intensive microcracking in mortar.

For mortar, the process of microcracking and crack development does not influence strongly AE spectrum – spectrum is more smooth than for concrete, and high-frequency components appear more often through the whole spectrum. The observation of AE events depends strongly on the initial parameters of the equipment used to test. For the wide-range B&K set-up with the sensor 8312, "graphite test" was used for sensor calibration. Results are presented in Fig.6. It can be seen, that optimum test conditions were for the amplification factor of $70dB$, and the filter of 200 kHz. For these parameters, signal was strong enough from the whole observation area, and at the same time, signals coming from the FPZ of the second crack were effectively eliminated.

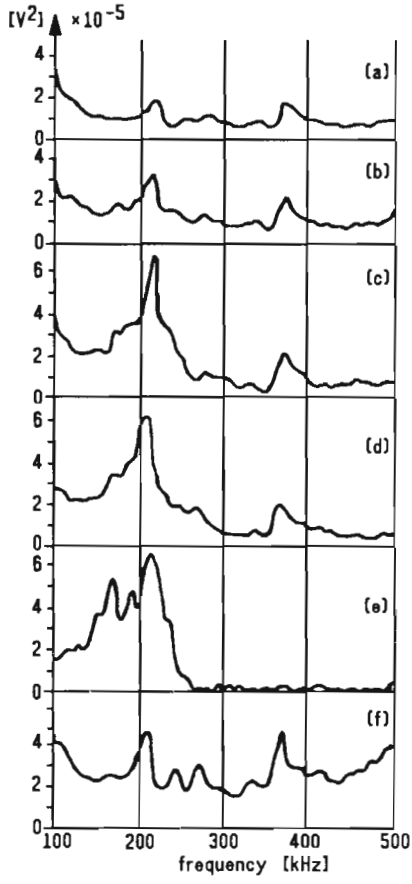

Fig. 5. AE spectrum for various cases of material degradation

7. Fracture toughness parameters for RC beams

Analytical formulae for K_I in the case of beams with a central crack, under four-point bending are derived according to well known mathematical techniques of fracture mechanics (cf Rooke et al., 1981). One should keep in mind the important restriction concerning boundary conditions: the crack edges should always be separated along their entire length. This is not the case for RC beams, where reinforcement prevents crack surfaces spacing.

This class of problems can be treated by the superposition technique. Complex configurations are considered to be a combination of separate, simpler configurations with separate boundary conditions. The stress intensity factors

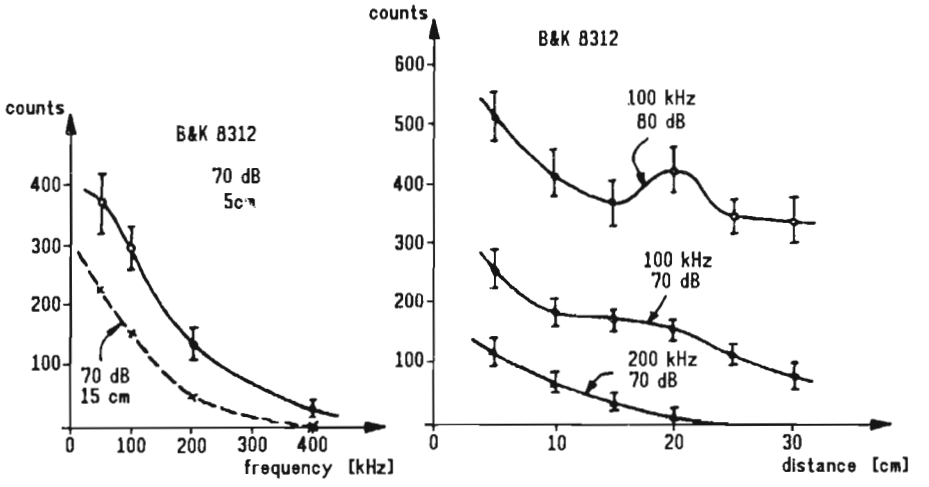

Fig. 6. Reaction of the B&K set-up for impulses from "graphite test"

(SIF) for simpler configurations are then added together to obtain the final solution. For modelling the action of reinforcement an approximate solution for a band of tension having variable width and acting over a part of the crack edge may be used (cf Rooke et al., 1981). A superposition technique was also successfully applied by Carpinteri (1986), who derived the complex SIF for a single edge crack subject to a bending moment and an axial force.

Another method available for determination of the fracture toughness parameters for RC beams is a compliance calibration. It is a general approach in treating complicated crack configurations and may be applicable to multi-cracks problems (cf Sundara Raja Iyengar et al., 1989). The basic equation is expressed in term of the strain energy release rate

$$G_I = \frac{P^2}{2b} C'(a) \tag{7.1}$$

where

C – compliance function of the specimen

$C'(a)$ – first derivative of a compliance function with respect to the crack length.

Compliance may be simply defined as

$$C = \frac{\delta}{P} \tag{7.2}$$

where δ is the displacement of the loading point. Finally, we may write

$$G_I = \frac{P}{2b}\delta'(a) \tag{7.3}$$

According to the basic relation of fracture mechanics K_I and G_I may be related as follows (for plane stress conditions)

$$G_I = \frac{K_I^2}{E} \tag{7.4}$$

The main problem is: how to evaluate the elastic moduli of concrete, which should reflect material degradation in the FPZ (cf Azad et al., 1987).

Evaluating either G_I or K_I requires $\delta'(a)$ value computation, which is often determined as the slope of the curve δ vs relative crack length a/h.

The relation $\delta - a/h$ was evaluated experimentally due to the testing procedure described above. The effective values of crack length provided by the photoelastic coating method had been applied to compliance calibration. Only the set of data for central crack (A) had been used for G_I evaluation. The compliance curves for three beams are shown in Fig.7.

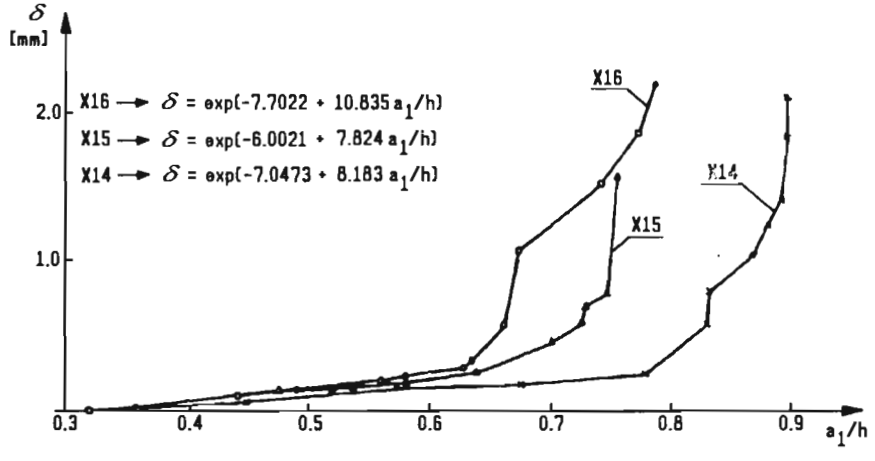

Fig. 7. Compliance curves for beams X14, X15, X16

They were approximated by the exponential function in the form

$$\delta = e^{[\alpha+\beta(a/h)]} \tag{7.5}$$

Particular expressions are given in Fig.7. Finally, it was possible to derive the G_I parameter as a function of different crack length, for various percentage of

reinforcement μ. The energy release rate characterize a composite fracture energy and takes into account the energy dissipation per unit crack extention for a particular reinforcement. In Fig.8 variation of G_I with respect to a/h and μ is presented for each beam.

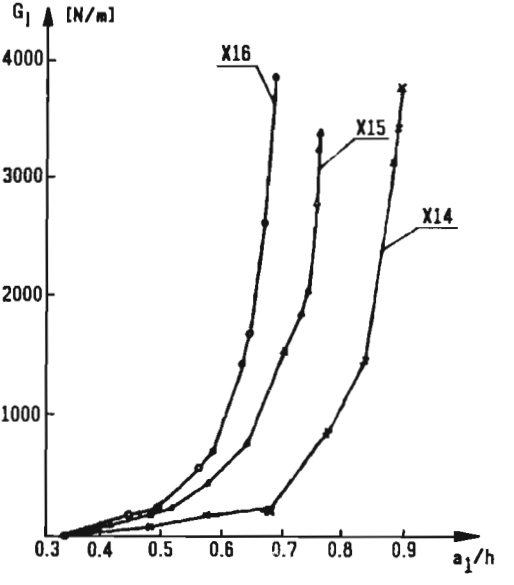

Fig. 8. Variation of G_I as a function of a/h and μ

8. Conclusions

Photoelastic coating method enables the observation of fracture process and enlargement of the microcracking zone in the crack tip area in concrete. It is also very convenient for monitoring interaction between cracks, what is expressed in terms of changes in isochromatic fringe configurations, and redistribution of strain field in the vicinity of the singularity point. Nevertheless, the fracture process in concrete composite, which is very complex in nature and develops stepwise calls for more accurate methods. Acoustic emission technique provides a tool for separation of the fracture phenomena and even for a numerical analysis of fracture in concrete – like composite. Certainly, more comprehensive experimental works are needed with the application of more accurate instrumentation.

The "effective" crack length, including FPZ at the crack tip, was the basis for evaluation of the modified strain energy release rate G_I for reinforced concrete. It characterizes the fracture process in RC members in terms of energy consideration. In the final stages of crack propagation the G_I value exceeds 4000 N/m, what is two orders of magnitude more, than fracture energy G_I^* for plain concrete (approximately 100 N/m). At the beginning of the FPZ formation $(a/h < 0.5) G_I$ is well below the level of 200 N/m and may be attributed to the fracture energy of plain concrete. With the expansion of crack the component of fracture energy connected with reinforcement strongly dominates the fracture process. It is evidently influenced by the amount of reinforcement – for $a/h = 0.7$ and for beam X16 $G_I = 7800$ N/m, for X15 $G_I = 1550$ N/m and for X14 $G_I = 220$ N/m.

References

1. AZAD A.K., BALUCH M.H., ZIRABA Y., 1987, *Fracture characterization of reinforced concrete beams,* SEM/RILEM Int.Conf.on Fract.of Concrete and Rock, Houston-Texas, June
2. CARPINTERI A., 1986, *Mechanical damage and crack growth in concrete. Plastic collapse to brittle fracture,* Martinus Nijhoff Publishers, Dordrecht-Boston-Lancaster
3. CEDOLIN L., DEI POLI S., IORI I., 1983, *Experimental determination of the fracture process zone in concrete,* Cem.Concr.Res., 13, 557-567
4. ENTOV W.M., JAGUST W.I., 1975, *Experimental investigation of the quasistatic microcracks development in concrete,* (in Russian), Mech.Tv.Tela, **10**, 93-103
5. GLUCKLICH J., 1963, *Fracture of plain concrete,* J.Eng.Mech.Div. ASCE EMG, 127-139
6. GODYCKI-ĆWIRKO T., 1982, *Mechanika betonu,* (in Polish), Arkady, Warszawa
7. INGRAFFEA A.R., SAOUMA V., 1986, *Numerical modelling of discrete crack propagation in reinforced and plain concrete,* Fracture Mechanics of Concrete, ed. Sih and Di Tommaso, Martinus Nijhoff Publishers, 95-140
8. JANKOWSKI L.J., STYŚ D.J., 1990, *Formation of the fracture process zone in concrete,* Eng.Fract.Mech., **36**, 2, 245-253
9. LIM M.K., KOO T.K., 1989, *Acoustic emission from reinforced concrete beams,* Mag.of Concr.Res., 41, 149, 229-234
10. MAJI A., OUYANG C., SHAH S.P., 1990, *Fracture mechanisms of quasi-brittle materials based on acoustic emission,* J.Mater.Res., **5**, 1, 206-217
11. MAJI A., SHAH S.P., 1988, *Process zone and acoustic-emission measurement in concrete,* Exp.Mech., 27-33

12. MAZARS J., 1981, *Mechanical damage and fracture of concrete structures,* Adv.Fract.Mech. – ICF 4, Cannes, 1499-1506

13. ROOKE D.P., BARATTA F.I., CARTWRIGHT D.J., 1981, *Simple methods of determining stress intensity factors,* Eng.Fract.Mech., 14, 397-426

14. ROSSI P., ROBERT J.L., GERVAIS J.P., BRUHAT D., 1990, *The use of acoustic emission in fracture mechanics applied to concrete,* Eng.Fract.Mech., **35**, 4/5, 751-763

15. SHAH, CARPINTERI, EDIT., 1991, *Fracture Mechanics Test Method for Concrete,* Report of Technical Committee 89-FMT Fracture Mechanics of Concrete: Test Methods., Chapman and Hall, London

16. SUNDARA RAJA IYENGAR K.T., RAGHUPRASAD B.K., ANANTHAN H., 1989, *Effect of interaction of macrocracks on the stress intensity factor in a beam,* Eng.Fract.Mech., **32**, 3, 379-386

17. SWARTZ S.E., GO C.G., 1984, *Validity of compliance calibration to cracked concrete beams in bending,* Exp.Mech., 24, 129-134

18. TERRIEN M., 1980, *Emission acoustique et "compartement mecanique postcritique" d'un beton sollicite en traction,* Bull. Liaison Lab. P. et Ch., 105, 65-72

Rozwój pęknięć w belkach betonowych

Streszczenie

W pracy przedstawiono wyniki badań rozwoju pęknięć i związanych z nimi obszarów FPZ w belkach betonowych zbrojonych pojedyńczym prętem stalowym. Pelnowymiarowe belki konstrukcyjne zawierające po dwie szczeliny obciążono stałym momentem i obserwowano rozwój pola odkształceń podczas ruchu szczelin przy zastosowaniu techniki warstwy elastooptycznej. Równocześnie podano emisję akustyczną poszczególne zdarzenia emisyjne i widmo sygnału.

Manuscript received October 1, 1993; accepted for print October 14, 1993